Performance of the HSDM model to predict competitive uptake of PFAS, NOM and inorganic anions by suspended ion exchange processes

Fuhar Dixit[a], Benoit Barbeau[b], Kim Maren Lompe[b], Ataollah Kheyrendish[a] and Madjid Mohseni[a]*

[a] Department of Chemical and Biological Engineering, University of British Columbia, Vancouver, Canada

[b] Department of Civil, Geological and Mining Engineering, Polytechnique Montreal , Quebec, Canada

Supplementary Information

S.1 Long- and short-chained perfluoroalkyl acids

According to the Organization of Economic Co-operation and Development (OECD 2013) PFAS are categorized as:

Long chained carboxylic acid PFAS: $C_nF_{2n+1}COOH$, $n \geq 7$ S.1.1

Long chained sulphonic acid PFAS: $C_nF_{2n+1}SO_3H$, $n \geq 6$ S.1.2

The rest are all short-chained carboxylic / sulphonic acid PFAS, as mentioned in Table 1.1[1,2].

Table S.1 Common Short- and Long-Chained PFCAS and PFSAS

Short-chained carboxylic acid PFAS					Long-chained carboxylic acid PFAS				
PFBA		PFPeA	PFHxA	PFHpA	PFOA	PFNA	PFDA	PFUnA	PFDoA
PFBS		PFPeS	PFHxS	PFHpA	PFOS	PFNS	PFDS	PFUnS	PFDoS
Short-chained sulphonic acid PFAS			Long-chained sulphonic acid PFAS						
Carbon atoms	4	5	6	7	8	9	10	11	12

S.2 LC-OCD data for natural waters

LC-OCD was performed using HPLC (Perkin Elmer, Canada) with 900 Turbo Potable OC Analyzer (detection range: 0.2-10 mg C/L, GE Sievers, Canada) for analysis of the source water NOM using a previously described method [3,4].

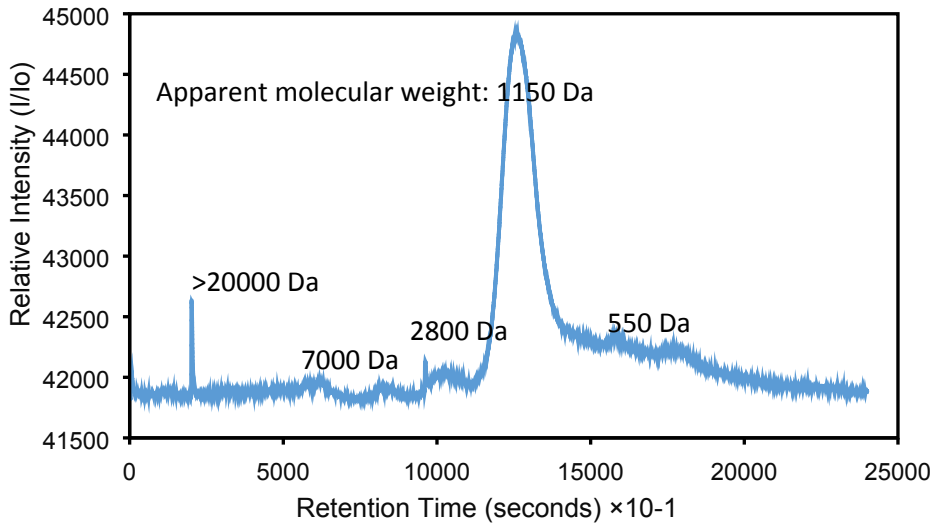

Figure S.1 LCOCD data for Vancouver Convention Centre Water before IX treatment

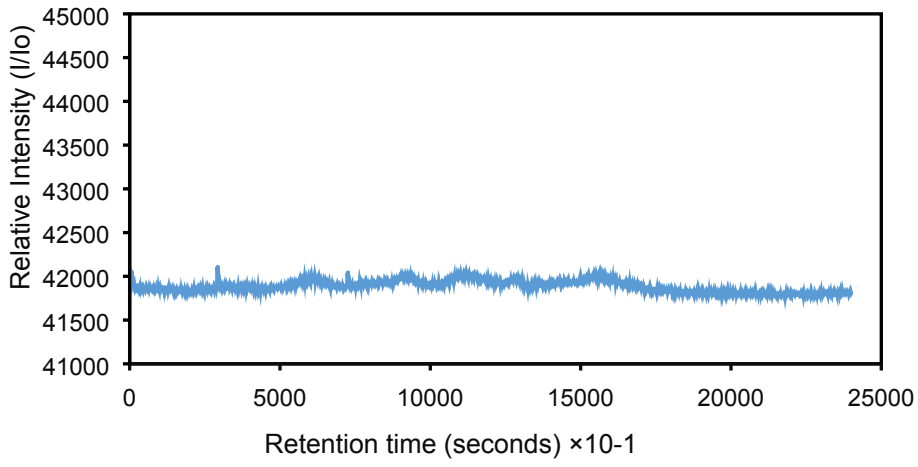

Figure S.2 LCOCD data for Vancouver Convention Centre Water after IX treatment (IX: 500 mg/L, 24 hours).

S.3 Vancouver convention centre (VCC) plant

The VCC treatment process comprises of a bacterial nutrient removal process followed by a treatment with a membrane bioreactor. The plant treats grey and black water from the building at an operating capacity of 100,000 Liters/day. The treated water is used in the washrooms for toilet flushing and rooftop irrigation during summer and warmer months. The process schematic can be observed in Figure S.3.

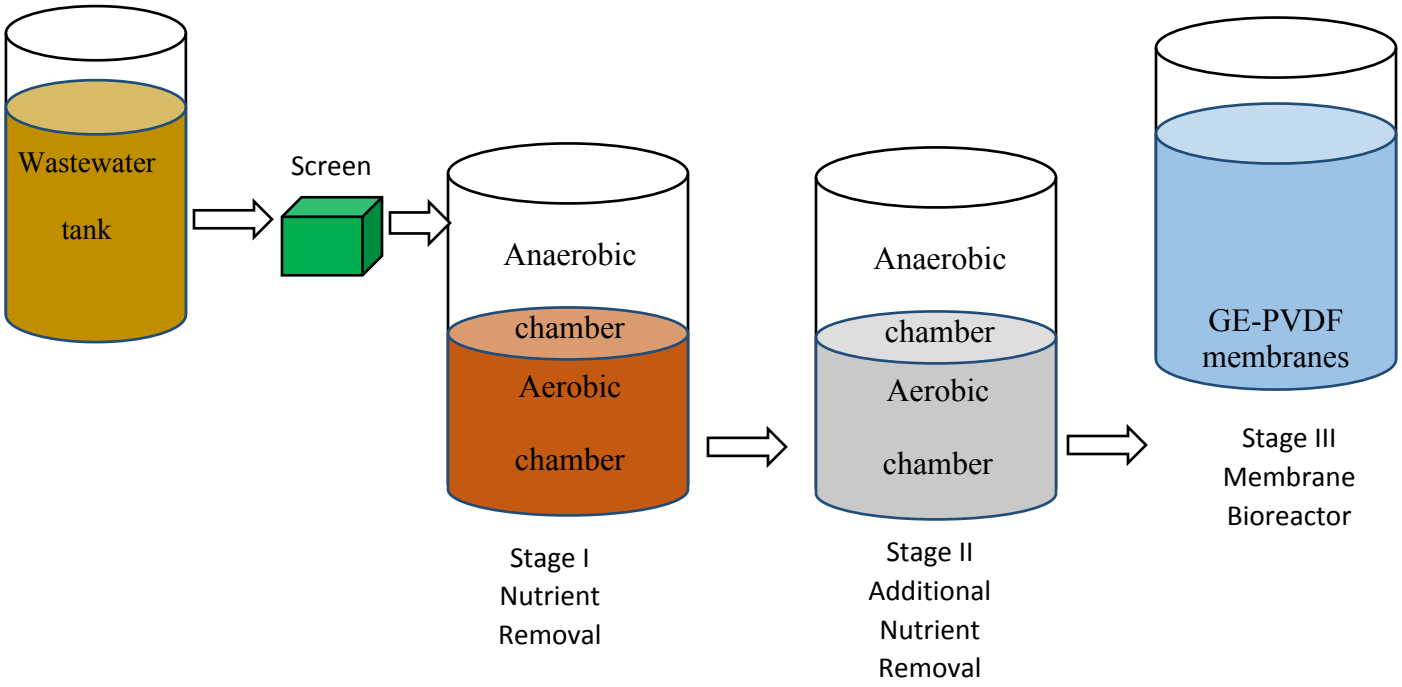

Figurer S.3 Schematic of the process flow at the Vancouver Convention Centre (VCC) secondary wastewater treatment plant.

S.4 Comparison of SRNOM and natural surface waters

As depicted in Figure S.3 and Figure S.4, both SRNOM containing water and water from a natural drinking water source in British Columbia (Middle River, previously adopted for surface water studies[5]) exhibit a similar range of molecular weight distribution with averages around 1050 Da[3,5].

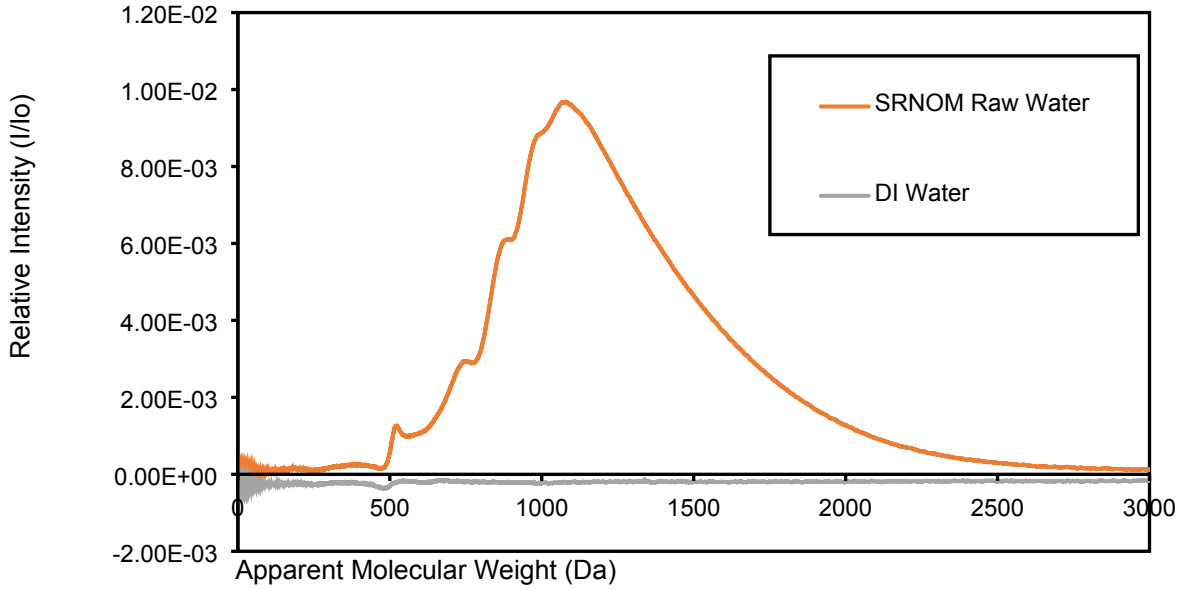

Figure S.4 LCOCD data for Suwanee River NOM (X-axis plotted with apparent molecular weight).

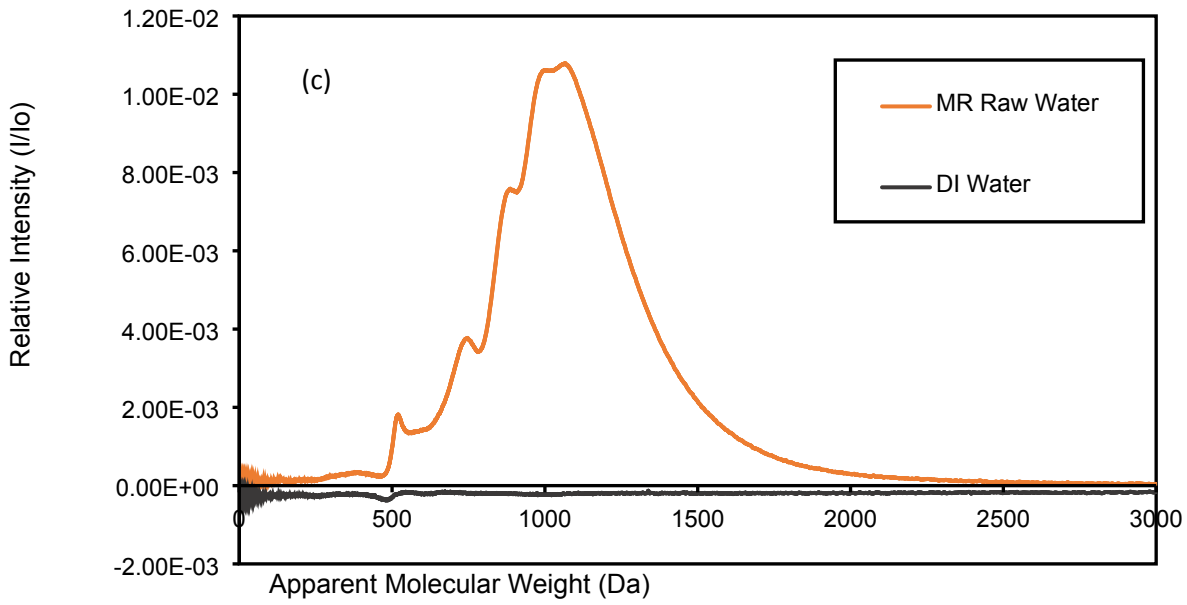

Figure S.5 Raw water characteristics Middle River Water (Natural surface water, BC, Canada)

S.5 Resin micro porosity data

Table S.2 depicts the resin porosimetry results (based on a mercury assay) for IX resin (Purolite A860) [3]. Considering the resin size range of 300-1200 μm[6], for modelling estimations, we assumed an average resin diameter of 750 μm (375 μm radius) as previously described [7].

Table S.2 Resin porosimetry results (based on a mercury assay) for Purolite A860

Pore Size	Cumulative Pore Area (m^2/g) × 10^{-3}	Pore Volume (mL/g) × 10^{-2}	Pore Area (%)	Pore Volume (%)
Macropores (>50 nm)	1.0	3.1	< 0.1	18
Mesopores (2-50 nm)	5.3	4.3	25.3	26
Micropores (<2nm)	15.6	9.0	74.6	56

S.6 Multicomponent EBC

The multicomponent interactions were further investigated as [8]:

$$(C_{i,0} - q_i C_{IX}) - \frac{q_i}{\sum_{j=1}^{N} q_j}\left(\frac{\sum_{j=1}^{N} n_j q_j}{n_i K_i}\right)^{n_i} = 0\ ,\ i = 1....N \qquad \text{S.6.1}$$

where subscript *i* represents the target component, *N* is the number of components (e.g., in a binary system, *N* =2, *i* = 1 for PFAS, and *i* = 2 for EBC), K_i and n_i represent the single-solute Freundlich constants, $C_{i,0}$ is the initial concentration of component *i* (μeq/L), C_{IX} is the IX dosage (meq/L) and q_i is the solid phase concentration (μmol/meq)[9].

For instance in a binary system, with e.g. only PFAS in presence of Suwannee River NOM, we get the following expressions:

$$C_{1,0} - q_1 C_{IX} - \frac{q_1}{q_1 + q_2}\left(\frac{n_1 q_1 + n_2 q_2}{n_1 K_1}\right)^{n_1} = 0 \qquad \text{S.6.2}$$

$$C_{2,0} - q_2 C_{IX} - \frac{q_2}{q_1 + q_2}\left(\frac{n_1 q_1 + n_2 q_2}{n_1 K_2}\right)^{n_2} = 0 \qquad \text{S.6.3}$$

As shown in equations S.6.2 and S.6.3, besides the adsorption parameters for the target compound ($C_{1,0}$, K_1 and n_1), three more EBC parameters ($C_{2,0}$,K_2 and n_2) are needed for the model prediction. These EBC parameters can be acquired using a non-linear optimization algorithm that could simultaneously solve the IAST equations as previously described [10,11]. In summary, solving the

model is started with estimated initial values and by assigning a small step change that can be added in recurring loops until the desired set of values fit the model within a range of permissible error (predefined value of say 0.01% error).

To evaluate the difference between model predictions and experimental data Marquardt's percent standard deviation (MPSD) [12] was used to predict the equilibrium adsorption data:

$$MPSD = 100\sqrt{\frac{1}{m-p}\sum_{i=1}^{p}\left(\frac{q_e\text{exp} - q_e cal}{qexp}\right)^2} \qquad \text{S.6.4}$$

where m is the number of experimental measurements and p is the number of parameters in the competitive isotherm. A smaller MPSD value (generally <10) corresponds to a better fit and lower error for the respective isotherm.

Note, the MPSD error which relates to the error of experimental data and model predictions should not be confused with the error value (say the 0.01%) previously defined to obtain EBC values during non-linear programming. The error value (of e.g. 0.01%) is used only to get the best possible values for the three EBC parameters that can fit the model with least error (here 0.01%). You may assign 0.001 % over 0.01% to get even better fits, it would just incur longer program runs to get the specified values.

S. 7 HSDM model

The governing equations of HSDM are illustrated below [13,14].

$$\frac{\partial q}{\partial t} = \frac{1}{r^2}\frac{\partial}{\partial R}\left(r^2 D_s \frac{\partial q}{\partial r}\right) \quad \text{S.7.1}$$

Where, r indicates the radial coordinate, q is the local concentration of PFAS in the ion exchange resin (neq/meq) and D_s is the surface diffusion coefficient (cm^2/s). If we assume the following boundary conditions:

$$C = C_0 \text{ and } q = 0 \text{ at } t = 0 \quad \text{S.7.2}$$

$$0 \le r \le 0.375 \ (R_p \text{ in cm}) \quad \text{S.7.3}$$

Assuming the radius of the resin (R_p) to be 0.375 cm (assumed spherical), we define the following initial and boundary conditions:

$$\frac{\partial q}{\partial r} = 0 \quad \text{For } t > 0 \text{ and } r = 0 \quad \text{S.7.4}$$

$$\rho D_p \frac{\partial q}{\partial r} = k_f\left(C_t - C_e\right) \quad \text{for } t > 0 \text{ and } r = R_p \quad \text{S.7.5}$$

$$Mass\ flux = \rho_p D_p \frac{\partial q}{\partial r} \quad \text{S.7.6}$$

$$\rho D_p \frac{\partial q}{\partial r} = k_f \left(C_0 - \frac{m}{v} \frac{3}{R_p^3} \int_0^{R_p} r^2 q dr - \left(\frac{q_S}{k_F} \right)^{1/n} \right) \quad \text{S.7.7}$$

C_o. C_t and C_e are concentrations of solute (mg/L) at time t = 0, at time t, and at equilibrium, respectively. k_f (cm/s) is the mass transfer coefficient ($k_f = D_f/\delta$). D_f (cm^2/s) is the film diffusion coefficient assuming δ film thickness of ~ 10^{-3} cm according to [15]. ρ is the density of the resin particle. Assuming the mass flux inside the resin as (equation S.7.6.), the conditions simplify to equation S.7.7, which can be utilized to predict the film and surface diffusion coefficients under the tested conditions (m is the resin dosage (meq/L) and v is the sample volume,

Equilibrium data in this study have shown that Freundlich adsorption isotherm agrees well with the experimental data.

$$q_e = k_F C_e^n \quad \text{S.7.8}$$

Therefore the governing equation 1 may be re expressed as

$$\frac{\partial q}{\partial t} = D_s \frac{\partial^2 q}{\partial r^2} + D_s \left(2 \frac{\frac{\partial q}{\partial r}}{r} \right) \quad \text{S.7.9}$$

At the centre of the adsorbent (r = 0). Hence,

$$\lim_{r \to 0} \left(\frac{\frac{\partial q}{\partial r}}{r} \right) = \frac{0}{0} \quad \text{S.7.10}$$

Applying L'Hospital's rule, we get

$$\lim_{r\to 0}\left(\frac{\frac{\partial q}{\partial r}}{r}\right)=\left(\frac{\frac{\partial^2 q}{\partial r^2}}{1}\right) \qquad \text{S.7.11}$$

This gives a modified equation after performing mass balances.

$$\frac{\partial q}{\partial t}=3D_s\frac{\partial^2 q}{\partial r^2} \qquad \text{S.7.12}$$

The equation S.7.12 may be represented as following in its dimensionless form [16]

$$\frac{\partial Y}{\partial T_B}=\frac{1}{R^2}\frac{\partial}{\partial x}\left(R^2\frac{\partial Y}{\partial R}\right) \qquad \text{S.7.13}$$

While equation S.7.5 in its dimensionless form could be represented as following:

$$\frac{\partial Y}{\partial R}=B_i(X-X_s) \qquad \text{S.7.14}$$

Here we define the dimensionless variable as:

$Y = q/q_o$ S.7.15

$X = C/C_o$ S.7.16

$X_f = C_f/C_o$ S.7.17

$R = r/R_p$ S.7.18

The dimensionless mass transfer Biot number (Bi), which is the ratio of internal mass transfer (i.e., surface diffusion) to external mass transfer (i.e., film diffusion) resistances can also be estimated, as previously described [3,7].

$$Bi=\frac{k_f R_p}{D_s} \qquad \text{S.7.19}$$

Here k_f (cm/s) is the external mass transfer coefficient ($k_f = D_f/\delta$), R_p is the radius of the ion exchange bead (0.375 cm), D_s is the surface diffusion coefficient (cm^2/s), D_f is the film diffusion coefficient (cm^2/s), δ is the film thickness (posed as 10^{-3} cm [7]). If the Biot number is high (>1), then the external mass transfer resistance may be ignored and only the internal surface diffusion comes into play, making the process limited by surface diffusion. Assuming a well-mixed system (150 rpm [7]), the empirical equation S.7.20 was used to describe solutions to the HSDM for an ion exchange system in a completely mixed batch reactor [17].

$$\frac{C - C_e}{C_0 - C_e} = A_0 + A_1(ln\text{ţ}) + A_2(ln\text{ţ})^2 + A_3(ln\text{ţ})^3 \quad 12$$

$$\text{ţ} = \frac{tD_s}{R_p^2} \quad 13$$

The constants A_0 to A_3 are tabulated for a range of $1/n$ values (solved using MATLAB [17]).

Approach: In order to find the HSDM parameters for a batch reactor, the HSDM imperial equation was fitted on the experimental data to find A0, A1, A2, and A3. Both Matlab's Levenberg-Marquardt toolbox and the curve-fitting toolbox was used to find the constant coefficients. Curve fitting toolbox delivered a faster and more accurate fitting compared to Levenberg-Marquardt toolbox by providing R-squares greater than 0.99 for PFOA, PFOS, PFBA, and PFBS.

S.8 Pseudo-second order kinetic model

The pseudo-second order kinetic model which considers that the rate is directly proportional to the number of active sites is given as [18–20]:

$$\frac{t}{q_t} = \frac{1}{k_2 q_e} + \frac{t}{q_e} = {}^{1}/_{v_0} + {}^{t}/_{q_e}$$

where k_2 (meq/neq/min) is the pseudo-second order rate constant, t is the contact time (min), q_e and q_t are the amounts of adsorbed contaminant ions on the resins at equilibrium and time t and υ_0 represents the initial sorption rate (mmol/g/h).

S.9 PFAS uptake kinetics

Table S.3 Literature data on pseudo-second order kinetic rate constants for PFOS on various IX resins.

Resin Tested	IRA 67 [a]	IRA 958 [a]	IRA 96 [a]	IRA 900 [a]	IRA 400 [a]	IRA 410 [a]	IRA 910 [b]	A860 [c]	A592 E [c]	MIEX [d]
Estimated v_0 (g/mmol/h)	0.76	1.08	0.21	0.11	0.01	0.03	0.09	6.13	19.62	n.d.
Resin Dosage (g/L)	0.01	0.01	0.01	0.01	0.01	0.01	0.1	0.1	0.1	3*
Equilibrium Time (h)	48	48	80	120	160	160	120	0.5	0.1	0.3
Initial Concentration (mg PFOS/L)	200	200	200	200	200	200	250	0.01	0.01	0.3

[a] Adopted from [21].
[b] Adopted from [22].
[c] Adopted from [20].
[c] Adopted from [23].

* Estimated assuming 1 mL =0.22 g (or 221 mg = 1 mL).

References

(1) Zhang, C.; Yan, H.; Li, F.; Hu, X.; Zhou, Q. Sorption of Short- and Long-Chain Perfluoroalkyl Surfactants on Sewage Sludges. *J. Hazard. Mater.* **2013**, *260*, 689–699. https://doi.org/10.1016/j.jhazmat.2013.06.022.

(2) Taniyasu, S.; Kannan, K.; Man, K. S.; Gulkowska, A.; Sinclair, E.; Okazawa, T.; Yamashita, N. Analysis of Fluorotelomer Alcohols, Fluorotelomer Acids, and Short- and Long-Chain Perfluorinated Acids in Water and Biota. *J. Chromatogr. A* **2005**, *1093* (1–2), 89–97. https://doi.org/10.1016/j.chroma.2005.07.053.

(3) Dixit, F.; Barbeau, B.; Mohseni, M. Characteristics of Competitive Uptake between Microcystin-LR and Natural Organic Matter (NOM) Fractions Using Strongly Basic Anion Exchange Resins. *Water Res.* **2018**, *139*, 74–82.

https://doi.org/10.1016/j.watres.2018.03.074.

(4) Winter, J.; Wray, H. E.; Schulz, M.; Vortisch, R.; Barbeau, B.; Bérubé, P. R. The Impact of Loading Approach and Biological Activity on NOM Removal by Ion Exchange Resins. *Water Res.* **2018**, *134*, 301–310. https://doi.org/10.1016/j.watres.2018.01.052.

(5) Dixit, F.; Barbeau, B.; Mohseni, M. Removal of Microcystin-LR from Spiked Natural and Synthetic Waters by Anion Exchange. *Sci. Total Environ.* **2019**, *655*, 571–580. https://doi.org/10.1016/j.scitotenv.2018.11.117.

(6) Purolite. *Purolite® A860 for Removing Organic Matter from Water*; 2017.

(7) Bazri, M. M.; Mohseni, M. Impact of Natural Organic Matter Properties on the Kinetics of Suspended Ion Exchange Process. *Water Res.* **2016**, *91*, 147–155. https://doi.org/10.1016/j.watres.2015.12.036.

(8) Bunmahotama, W.; Hung, W. N.; Lin, T. F. Prediction of the Adsorption Capacities for Four Typical Organic Pollutants on Activated Carbons in Natural Waters. *Water Res.* **2017**, *111*, 28–40. https://doi.org/10.1016/j.watres.2016.12.033.

(9) Dixit, F.; Barbeau, B.; Mostafavi, S. G.; Mohseni, M. Removal of Legacy PFAS and Other Fluorotelomers: Optimized Regeneration Strategies in DOM-Rich Waters. *Water Res.* **2020**, *183*, 116098. https://doi.org/10.1016/j.watres.2020.116098.

(10) Crittenden, J. C.; Sanongraj, S.; Bulloch, J. L.; Hand, D. W.; Rogers, T. N.; Speth, T. F.; Ulmer, M. Correlation of Aqueous-Phase Adsorption Isotherms. *Environ. Sci. Technol.* **1999**, *33* (17), 2926–2933. https://doi.org/10.1021/es981082i.

(11) Najm, I. N.; Snoeyink, V. L.; Richard, Y. Effect of Initial Concentration of a SOC in

Natural Water on Its Adsorption by Activated Carbon. *J. Am. Water Works Assoc.* **1991**, *83* (8), 57–63. https://doi.org/10.1002/j.1551-8833.1991.tb07200.x.

(12) Kumar, K. V.; Porkodi, K.; Rocha, F. Comparison of Various Error Functions in Predicting the Optimum Isotherm by Linear and Non-Linear Regression Analysis for the Sorption of Basic Red 9 by Activated Carbon. *J. Hazard. Mater.* **2008**, *150* (1), 158–165. https://doi.org/10.1016/j.jhazmat.2007.09.020.

(13) Du, Z.; Deng, S.; Bei, Y.; Huang, Q.; Wang, B. Adsorption Behavior and Mechanism of Perfluorinated Compounds on Various Adsorbents — A Review. *J. Hazard. Mater.* **2014**, *274*, 443–454. https://doi.org/10.1016/j.jhazmat.2014.04.038.

(14) Worch, E. *Adsorption Technology in Water Treatment: Fundamentals, Processing and Modelling*; GmbH and Co. KG, Berlin/Boston, 2012.

(15) Helfferich, F. Ion-Exchange Kinetics. V. Ion Exchange Accompanied by Reactions. *J. Phys. Chem.* **1965**, *69* (4), 1178–1187. https://doi.org/10.1021/j100888a015.

(16) Muthukkumaran, A.; Aravamudan, K. Combined Homogeneous Surface Diffusion Model – Design of Experiments Approach to Optimize Dye Adsorption Considering Both Equilibrium and Kinetic Aspects. *J. Environ. Manage.* **2017**, *204*, 424–435. https://doi.org/10.1016/j.jenvman.2017.09.010.

(17) Crittenden, J. C.; Trussell, R. R.; Hand, D. W.; Howe, K. J.; Tchobanoglous, G. *MWH's Water Treatment*; John Wiley & Sons, Inc.: Hoboken, NJ, USA, 2012. https://doi.org/10.1002/9781118131473.

(18) Rengaraj, S.; Yeon, J.-W.; Kim, Y.; Jung, Y.; Ha, Y.-K.; Kim, W.-H. Adsorption

Characteristics of Cu(II) onto Ion Exchange Resins 252H and 1500H: Kinetics, Isotherms and Error Analysis. *J. Hazard. Mater.* **2007**, *143* (1–2), 469–477. https://doi.org/10.1016/j.jhazmat.2006.09.064.

(19) Sahetya, T. J.; Dixit, F.; Balasubramanian, K. Waste Citrus Fruit Peels for Removal of Hg(II) Ions. *Desalin. Water Treat.* **2013**, *3994* (February 2015), 1–13. https://doi.org/10.1080/19443994.2013.852483.

(20) Dixit, F.; Barbeau, B.; Mostafavi, S. G.; Mohseni, M. PFAS and DOM Removal Using an Organic Scavenger and PFAS-Specific Resin: Trade-off between Regeneration and Faster Kinetics. *Sci. Total Environ.* **2020**, 142107. https://doi.org/10.1016/j.scitotenv.2020.142107.

(21) Deng, S.; Yu, Q.; Huang, J.; Yu, G. Removal of Perfluorooctane Sulfonate from Wastewater by Anion Exchange Resins: Effects of Resin Properties and Solution Chemistry. *Water Res.* **2010**, *44* (18), 5188–5195. https://doi.org/10.1016/j.watres.2010.06.038.

(22) Maimaiti, A.; Deng, S.; Meng, P.; Wang, W.; Wang, B.; Huang, J.; Wang, Y.; Yu, G. Competitive Adsorption of Perfluoroalkyl Substances on Anion Exchange Resins in Simulated AFFF-Impacted Groundwater. *Chem. Eng. J.* **2018**, *348* (May), 494–502. https://doi.org/10.1016/j.cej.2018.05.006.

(23) Park, M.; Daniels, K. D.; Wu, S.; Ziska, A. D.; Snyder, S. A. Magnetic Ion-Exchange (MIEX) Resin for Perfluorinated Alkylsubstance (PFAS) Removal in Groundwater: Roles of Atomic Charges for Adsorption. *Water Res.* **2020**, *181*, 115897. https://doi.org/10.1016/j.watres.2020.115897.